Textures and Microstructures, 1993, Vol. 21, pp. 207–217
Reprints available directly from the publisher.
Photocopying permitted by license only

EVOLUTION OF TEXTURE AND YIELD LOCUS OF AISI 409 FERRITIC STAINLESS STEEL

N. MINGOLO and A. POCHETTINO

Depto. Materiales, Gerencia Desarrollo, CNEA, Av. Libertador 8250, 1429 Buenos Aires, Argentina

and

C. VIAL-EDWARDS

Escuela de Ingenieria, Pontificia Universidad Católica de Chile, Vicuña Mackenna 4860, Santiago, Chile

(Received March 10, 1993)

The evolution of texture and yield locus of AISI 409 ferritic stainless steel under different deformation paths was analyzed.

Texture evolution with plastic deformation was predicted by two models: Taylor (TPG), assuming pencil glide in {hkl}⟨111⟩ slip systems and Viscoplastic under the relaxed constraint assumption (VRC), considering the following slip systems: {110}⟨111⟩, {112}⟨111⟩, and {123}⟨111⟩, selected according to a strain rate sensitivity law. TPG model tends to predict some stronger developments of texture than the VRC model.

Predictions of stress–strain curves along different loading paths with TPG and VRC models were very close to experimental results. Texture evolution did not have a significant effect to modify the rate and the isotropy of the strain hardening process of AISI 409 ferritic stainless steel.

KEY WORDS Ferritic steel, yield locus, Taylor model, rate sensitive model

NOTATION

0°, 45°, 90°	angles to the rolling direction
ψ, θ, φ	angles in Euler space
τ_k	resolved shear stress on the k slip system
m	strain rate sensitivity exponent
$\dot{\gamma}^k$, $\dot{\gamma}_0^k$	shear strain rate and reference shear strain rate on the k slip system
τ^k, τ_0^k	resolved shear stress and reference resolved shear stress on the k slip system
τ_r	critical resolved shear stress
$\dot{\varepsilon}_{ij}$	strain rate tensor
ε_{eq}	equivalent strain
r_{ij}^k	symmetric part of the m_{ij}^k tensor, $m_{ij}^k = b_i^k \cdot n_j^k$
b_i^k	components of the slip vector
n_j^k	components of the normal to the slip plane
σ_n	stress tensor
$(-q)$	ratio of transverse to longitudinal strain

$\bar{M}$	average Taylor factor
$g(\psi, \theta, \varphi)$	grain orientation in Euler space
$f(g)$	Crystallite Orientation Function (ODF)
(U_0, U_{45}, U_{90})	flow stress in uniaxial tension tests at 0°, 45° and 90°
U_{av}	$(U_0 + U_{90} + 2U_{45})/4$
P_0, P_{90}	flow stress in quasi plane-strain tension tests
B	flow stress in biaxial tension test
R	Lankford anisotropy coefficient
k, n	parameters in equation $\sigma = K\varepsilon^n$

1. INTRODUCTION

The knowledge of the evolution of crystallographic textures by plastic deformation is important for modelling mechanical properties of metals; texture is related to the shape of the yield locus and to the elastic and plastic anisotropy. Taylor (1938) (TPG) and Viscoplastic (VRC) Canova *et al.* 1985 models were used to predict the evolution of crystallographic textures and stress–strain curves of an AISI 409 ferritic stainless steel sheet metal, plastically deformed along different loading paths. AISI 409 steel had the following chemical composition (wt.%): C: 0.03; S: 0.004; Al: 0.03; Si: 0.68; Cr: 11.5; Ti: 0.4. Predicted true stress-true strain curves were compared to experimental data obtained by the following mechanical tests: uniaxial tension along rolling (0°) and transverse (90°) directions; quasi plane-strain tension along 0° and 90° directions and biaxial tension. The evolution of the shape of the yield locus was analyzed by comparing yield stresses of material deformed by different loading paths, at the same level of plastic deformation energy.

2. ANALYSIS OF TEXTURE EVOLUTION

(a) *Description of Texture*

The texture of the material was represented by a discrete set of orientations with their corresponding weights. The initial texture of AISI 409 ferritic stainless steel was described by a set of 371 orientations in Euler space. This corresponds to a reduced representation of texture (Tomé *et al.* 1988) that neglects orientations whose volume fraction is smaller than a minimum value. Figure 1, shows good agreement between the reduced representation of texture and that determined from experimental pole figures. Texture analysis shows reinforcements around the following orientations: $\{233\}\langle 113\rangle$ ($\varphi = 45°$, $\theta = 65°$, $\psi = 0°$); $\{554\}\langle 225\rangle$ ($\varphi = 45°$, $\theta = 60°$, $\psi = 0°$) and $\{111\}\langle 112\rangle$ ($\varphi = 45°$, $\theta = 55°$, $\psi = 0°$ and 60°).

(b) *Prediction of Texture Evolution*

According to the classical methods to simulate texture evolution e.g. Arminjon (1987), the orientations were allowed to evolve during deformation while the associated volume fractions were kept constant. Two models were utilized to predict the evolution of texture, starting from the initial experimental texture

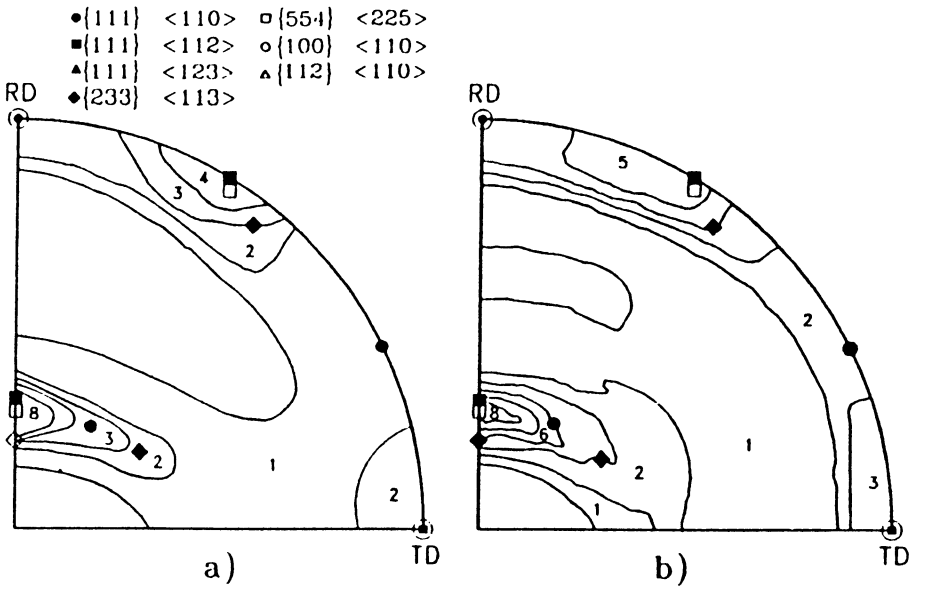

Figure 1 {110} pole figures corresponding to the as received AISI 409 ferritic stainless steel. (a) Complete set of orientations. (b) Reduced orientations.

shown in Figure 1b:

—Taylor model (TPG). TPG postulates that the strain is identical in all grains and equal to the external imposed strain; for ferritic stainless steel, pencil glide deformation on $\{hkl\}\langle 111\rangle$ slip systems and full constraint was assumed.

—Viscoplastic model under the relaxed constraints assumption (VRC). VRC considers that deformation is accommodated by $\{110\}\langle 111\rangle$, $\{112\}\langle 111\rangle$ and $\{123\}\langle 111\rangle$ slip systems. The shear strain rate on a slip system ($\dot{\gamma}^k$) is related to the corresponding resolved shear stress (τ^k) by Eq. (1):

$$\frac{\tau^k}{\tau_0^k} = \left(\frac{\dot{\gamma}^k}{\dot{\gamma}_0^k}\right)^m \tag{1}$$

where: m is the strain rate sensitivity exponent, $\dot{\gamma}_0^k$ and τ_0^k are reference shear strain rate and resolved shear stress respectively.

The relaxed condition hypothesis (Honneff and Mecking 1981) assumes that some components of stress (Sachs 1928) and some components of strain (Taylor) are imposed and the relaxed or free components are obtained by equation:

$$\dot{\varepsilon}_{ij} = \dot{\gamma}_0 \sum_k r_{ij}^k \left[\frac{\sum_{l,n} r_{ln}^k \cdot \sigma_{ln}}{\tau_0^k}\right]^{1/m} \tag{2}$$

where $\dot{\varepsilon}_{ij}$ is the strain rate tensor, r_{ij}^k is the symmetric part of the m_{ij}^k tensor ($m_{ij}^k = b_i^k \cdot n_j^k$), b_i^k and n_j^k are the components of slip vector and the normal to the slip plane respectively, σ_{ln} is the stress tensor. The strain state for each deformation path was described by the ε_{ij} tensor, with principal directions along

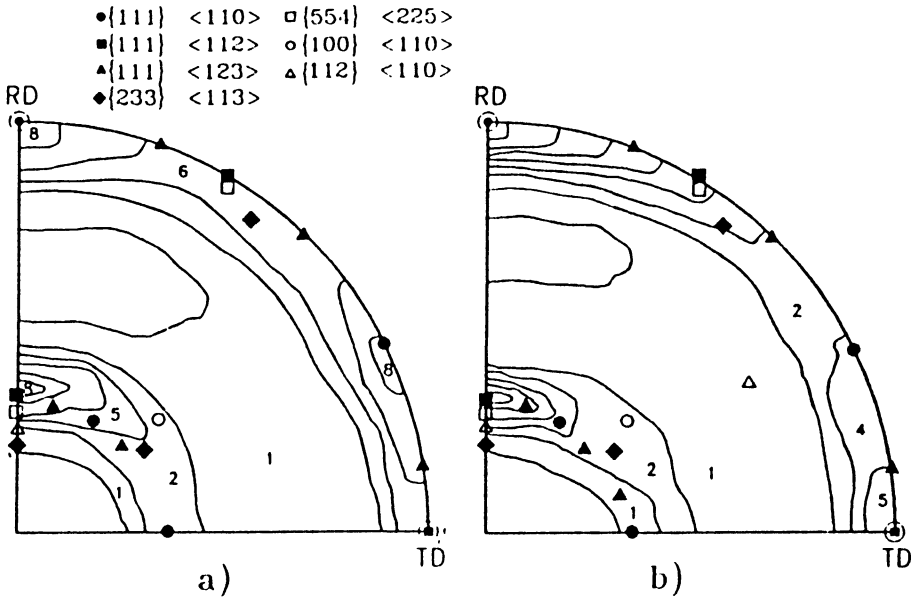

Figure 2 Predicted {110} pole figures for uniaxial tension along rolling direction, at $\varepsilon = 0.18$. (a) TPG model. (b) VRC model.

rolling (0°), transverse (90°) and normal directions; the ratio $(-q)$ of transverse to longitudinal strain was used to describe different loading paths.

Both models: TPG and VRC assumed isotropic hardening of the critical resolved shear stress τ_c with a strain hardening exponent equal to the one observed in uniaxial tension tests; the strain rate sensitivity exponent (m) defined by Eq. (1), takes values of 0 for TPG and 0.05 for VRC.

Figures 2 to 6 show pole figures predicted with the VRC and TPG models for material deformed—up to the indicated level of plastic strain—under: uniaxial tension (Figs. 2 and 3), quasi plane-strain tension (Figs. 4 and 5) and biaxial tension (Fig. 6).

The analysis of pole figures shows the following results:

—Uniaxial tension tests (Figures 2 and 3): the VRC and TPG models predict a reinforcement of the $\{111\}\langle 110\rangle$ and $\{111\}\langle 112\rangle$ texture components.

—Quasi Plane-strain tension tests (Figures 4 and 5): For rolling direction, both VRC and TPG models predict reinforcements of fiber components around: $\{111\}\langle 110\rangle$ and $\{111\}\langle 112\rangle$; $\{100\}\langle 110\rangle$ and $\{112\}\langle 110\rangle$. The TPG model predicts a strong reinforcement of the $\{111\}\langle 110\rangle$ and $\{112\}\langle 110\rangle$ components; the VRC model leads to a less sharper texture than the TPG model, a usual trend associated to the model (Mingolo 1990). The stability of the $\{554\}\langle 225\rangle$ component with deformation was also predicted. This result is in agreement with experimental textures corresponding to Ti-stabilized ferritic steels (Inagaki 1988). Texture evolution, for quasi plane-strain tests along transverse direction, shows the development of the $\{111\}\langle uvw\rangle$ fiber component, with a reinforce-

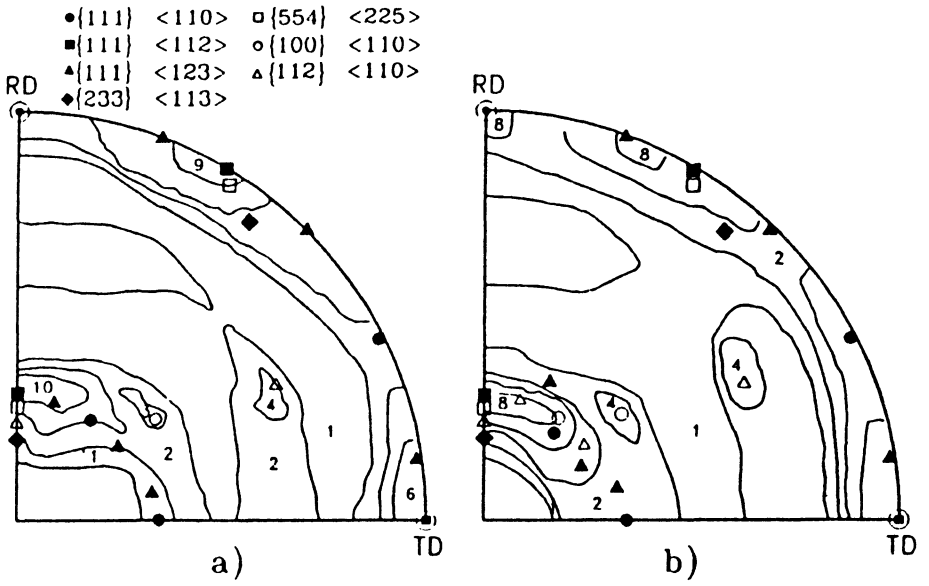

Figure 3 Predicted {110} pole figures for uniaxial tension along transverse direction, at $\varepsilon = 0.30$. (a) TPG model. (b) VRC model.

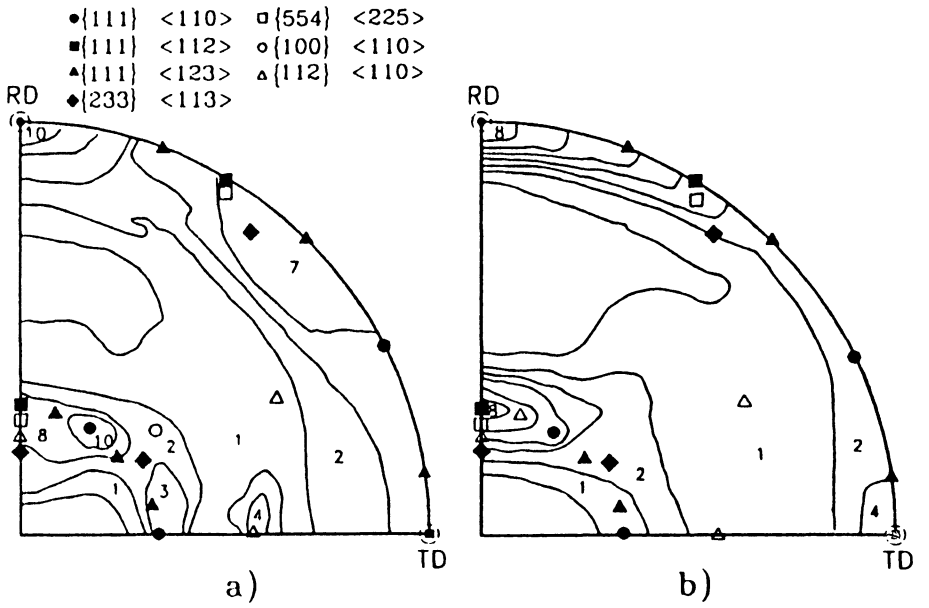

Figure 4 Predicted {110} pole figures for quasi-plane strain tension along rolling direction, at $\varepsilon = 0.23$. (a) TPG model. (b) VRC model.

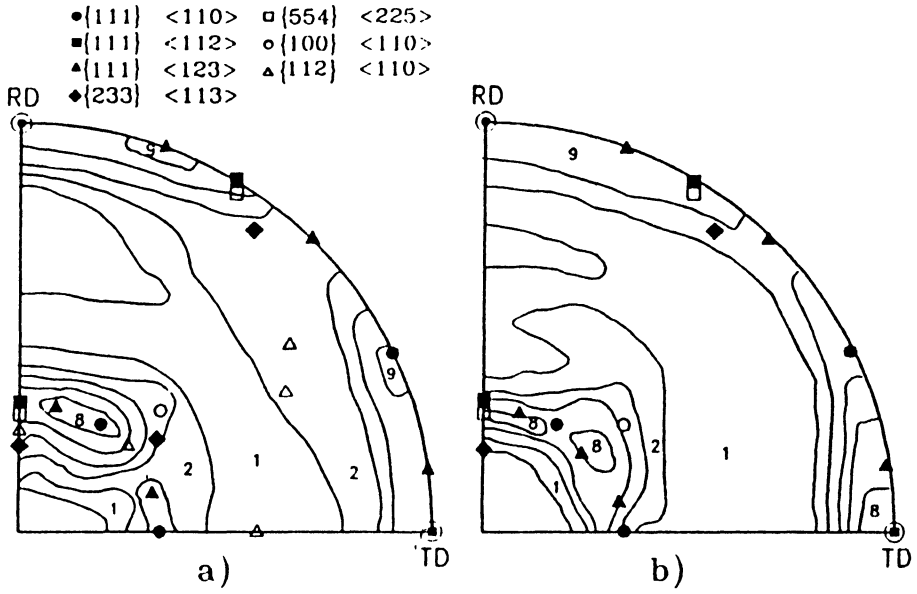

Figure 5 Predicted pole figures for quasi-plane strain tension along transverse direction, at $\varepsilon = 0.22$. (a) TPG model. (b) VRC model.

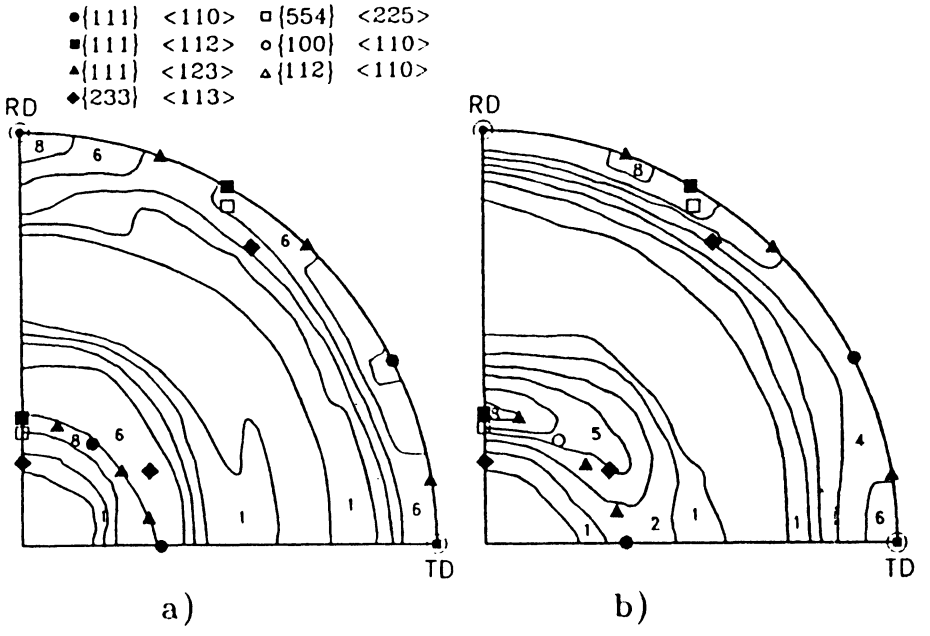

Figure 6 Predicted pole figures for uniaxial tension, at $\varepsilon = 0.20$ (deformation in the plane of the sheet) (a) TPG model. (b) VRC model.

ment around the $\{111\}\langle 110\rangle$, $\{111\}\langle 112\rangle$ and $\{111\}\langle 123\rangle$ components. The initial $\{554\}\langle 225\rangle$ component was also stable with deformation.

—Biaxial tension (Figure 6): the $\{111\}\langle uvw\rangle$ fiber component was reinforced, mainly around the $\{111\}\langle 112\rangle$ and $\{111\}\langle 110\rangle$ orientations. The texture predicted by the TPG model shows a tendency to complete the $\{111\}\langle uvw\rangle$ fiber texture.

3. PREDICTION OF THE EVOLUTION OF THE YIELD LOCUS

(a) *Description of the Yield Locus Utilizing Textural Data*

It is well known that the yield locus of a polycrystalline material is the envelope of hyperplans, which are tangent to it. Each hyperplane corresponds to an imposed strain state ε_{ij}. The following equation is verified in the stress space σ_{ij}:

$$\varepsilon_{ij}\sigma_{ij} = \tau_c \bar{M}(\varepsilon_{ij})\varepsilon_{eq} \tag{3}$$

where: τ_c is the critical resolved shear stress (CRSS) for slip, identical on all $\{hkl\}\langle 111\rangle$ systems; ε_{eq} is the equivalent strain $[\varepsilon_{eq} = (2/3\varepsilon_{ij}\varepsilon_{ij})^{1/2}]$ and $\bar{M}(\varepsilon_{ij})$ is the average Taylor factor.

Both models, TPG and VRC, predicted stress–strain curves along different loading paths assuming that τ_c increases isotropically with the strain hardening exponent determined in uniaxial tension tests; this assumption was based on the small variations shown by the "n" exponent of the different uniaxial tension curves (Table I).

For a textured specimen, the average Taylor factor is calculated by:

$$\bar{M}(\varepsilon_{ij}) = \int_g \bar{M}(\varepsilon_{ij}, g) f(g)\, dg \tag{4}$$

where: $\bar{M}(\varepsilon_{ij}, g)$ corresponds to the Taylor factor associated to a given grain orientation g, $f(g)$ is the Crystallite Orientation Function (ODF) and $f(g)$. dg defines the volume fraction of grains having an orientation $g(\psi, \theta, \varphi)$ in the Euler space. In the present work, the texture representation included a discrete number of orientations, then the integral was replaced by a sum over the different orientations of grains with their corresponding weights.

(b) *Predicted and Experimental Results*

The evolution of the Yield Locus was both calculated from the predicted evolution of textures and experimentally determined from stress–strain curves obtained by the following mechanical tests:

—Uniaxial tension along rolling and transverse directions (U_0, U_{90}), with standard tensile specimens.

—Quasi plane-strain tension with Wagoner type specimen (Wagoner 1980) along rolling and transverse directions (P_0, P_{90}). The Wagoner type specimen is short in the tensile direction and wide in the transverse direction, a state of quasi plane-strain is generated in most of the width of it, with the exception of both ends.

—Biaxial tension (B). The well known bulge test was employed, with a 5 in. diameter specimen.

Table I Experimental and predicted stress–strain curves

(a) *Experimental*			
Test	*K (MPa)*	*n*	*R*
U_0	819.5	0.217	1.24
U_{90}	809.5	0.222	1.28
U_{45}	806.7	0.235	1.35
U_{av}	806.7	0.227	
P_0	980.9	0.235	
P_{90}	1031.0	0.230	
B	938.0	0.213	

(b) *Predicted by TPG and VRC models*

	K (MPa)		*n*	
	TPG	*VRC*	*TPG*	*VRC*
P_0	1045	1047	0.271	0.256
P_{90}	1045	1046	0.233	0.229
B	948	973	0.203	0.209

Table I shows true stress-true strain curves represented by the parameters K and n, obtained by power law regression of equation: $\sigma = K\varepsilon^n$, R is the Lankford strain ratio. Experimental and predicted values—with TPG and VRC models—are included.

Table II shows stress ratios for different loading paths, compared at the same level of plastic deformation energy utilizing data from Table I. Three different levels of plastic strain in uniaxial tension were considered.

Figure 7 compares experimental true stress- true strain curves obtained in

Table II Stress ratios for experimental and predicted stress–strain curves

	P_0/U_0		
εU_0	*Experimental*	*TPG*	*VRC*
0.1	1.124	1.108	1.139
0.15	1.130	1.127	1.153
0.2	1.134	1.141	1.164
	P_{90}/U_{90}		
εU_{90}	*Experimental*	*TPG*	*VRC*
0.1	1.201	1.207	1.217
0.15	1.204	1.211	1.220
0.2	1.206	1.215	1.222
	B/U_0		
εU_0	*Experimental*	*TPG*	*VRC*
0.1	1.126	1.157	1.168
0.15	1.124	1.151	1.165
0.20	1.123	1.148	1.163

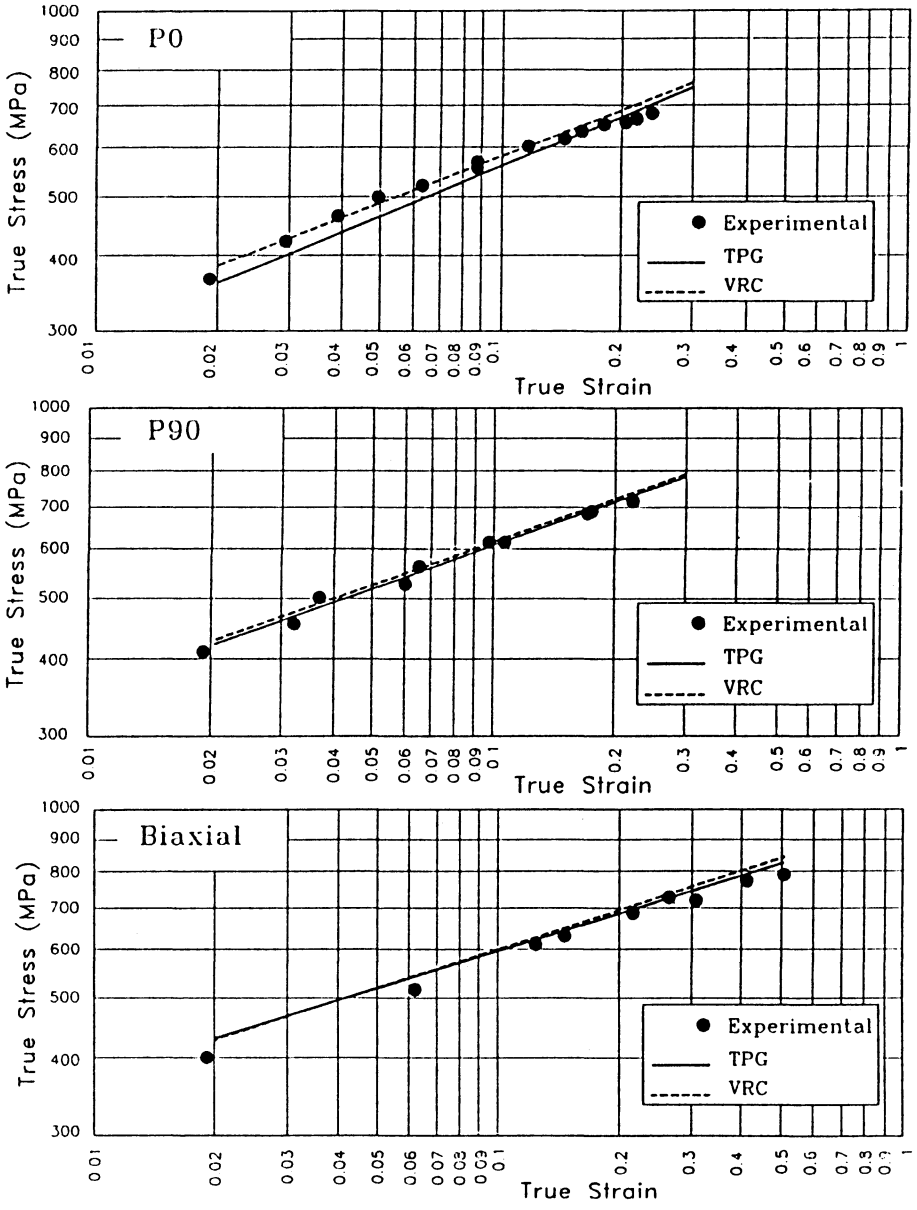

Figure 7 True stress-true strain curves. Experimental and predicted with TPG and VRC models. (a) P_0. (b) P_{90}. (c) Biaxial.

quasi-plane strain tension (P_0 and P_{90}) and biaxial tension (B) tests to predicted curves with TPG and VRC models (Table I).

(c) *Analysis of Results*

Experimental results (Table I) show isotropy in the plane of the sheet, uniaxial tension true stress-true strain curves and Lankford coefficients (R) have no significant variations at 0°; 90° and 45° to the rolling direction. Strain hardening exponents of quasi plane-strain (P_0 and P_{90}) and biaxial (B) curves do not differ significantly from corresponding in uniaxial tension. Experimental results show isotropic evolution of the yield locus.

Table I and Figure 7 show that TPG and VRC models give very similar predictions. The agreement between predicted and experimental results is very good for Biaxial and P_{90} data; for P_0, predicted curves lie close to the experimental data but predicted strain hardening exponents are somewhat higher than experimental exponents.

The evolution of texture produced by plastic deformation along different loading paths—included in predictions of stress–strain curves with TPG and VRC models through $\bar{M}(\varepsilon_{ij})$—did not have a significant effect to modify the rate and the isotropy of the strain hardening.

4. CONCLUSIONS

1. The use of a reduced representation of texture (371 orientations) produced a good agreement with experimental results obtained by the complete set of orientations.
2. The TPG model tends to predict some stronger developments of texture than the VRC model.
3. Predictions with TPG and VRC models of stress–strain curves under different loading paths were both very similar and close to the experimental curves.
4. Predictions with TPG and VRC models assumed isotropic hardening of the critical resolved shear stress with a strain hardening exponent equal to the one observed in uniaxial tension tests. Texture evolution, included in the different predictions of the stress–strain curves through the $\bar{M}(\varepsilon_{ij})$ factor, did not have a significant effect to modify the rate and the isotropy of the strain hardening process for AISI 409 ferritic stainless steel.

Acknowledgements

We wish to thank the support received by: Departamento de Materiales de la Comisión de Energía Atómica, Argentina; Multinational Project of Materials, American States Organization and project 91-0765 FONDECYT, CONICYT-CHILE.

References

Arminjon, M. (1987), *Acta Metall.*, **3,** 615.
Canova, G. R., Kocks, U. F., Tomé, C. N. and Jonas, J. J. (1985), *J. Mech. and Phys. Solids*, **33,** 371.
Honneff, H. and Mecking, H. (1981), *Proc. ICOTOM* **6,** 347.
Inagaki, H. (1988), *Textures and Microstructures,* **8,** 173.
Mingolo, N. (1990), Ph.D. Thesis University of Buenos Aires.
Sachs, G. (1928), *Z.V. Deut. Ing.*, **72,** 734.
Taylor, G. I. (1938), *Institute of Metals,* **62,** 307.
Tomé, C., Pochettino, A. and Penelle, R. (1988), *Proc. ICOTOM* **8,** The Metallurgical Soc., 1059.
Wagoner, R. H. (1980), *Metallurgical Transactions A,* **11A,** 165.